Reactive and Functional Polymers 190 (2023) 105635

Contents lists available at ScienceDirect

Reactive and Functional Polymers

journal homepage: www.elsevier.com/locate/react

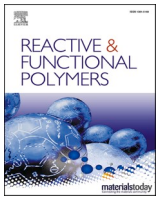

Effects of cryogenic condition and chemistry on the properties of synthetic and biopolymer cryogels

Gamze Doser [a], Esra Su [b], Oguz Okay [a,*]

[a] Istanbul Technical University, Department of Chemistry, Maslak, 34469 Istanbul, Turkey
[b] Istanbul University, Faculty of Aquatic Sciences, Aquatic Biotechnology, Fatih, 34134 Istanbul, Turkey

ARTICLE INFO

Keywords:
Cryogels
Macroporous polymers
Cryogelation
Porosity
Cryoconcentration

ABSTRACT

We discuss here the properties of seven different synthetic and biopolymer cryogels prepared under identical conditions, and how the cryogenic condition and chemistry affect their properties. The monomers used in the study are acrylamide (AAm), *N*, *N*-dimethylacrylamide (DMAA), sodium acrylate (NaAA), sodium methacrylate (NaMA), and 2-acrylamido-2-methylpropane sulfonic acid sodium salt (AMPS). Silk fibroin (SF), and double-stranded deoxyribonucleic acid (DNA) are selected as the biopolymers for the preparation of the cryogels. The nonionic monomers AAm and DMAA produce cryogels with the largest total pore volumes and average pore diameters while ionic cryogels exhibit a small pore volume due to the collapse of the pores during their drying. Moreover, SF cryogel has the most mechanically stable porous structure followed by AAm and DMAA cryogels. The experimental findings can be explained with the cryogenic conditions namely, the total ice volume in the cryogelation system and the true concentration of the monomers or polymers in the unfrozen domains after cryoconcentration, as determined from DSC measurements. The extent of cryoconcentration and hence the true concentration of the monomers or polymers regulate the mechanical stability of the cryogel pore walls.

1. Introduction

Cryogelation is a simple and green technique to produce mechanically robust, fast responsive, macroporous hydrogels, so-called cryogels [1–5]. The key point of this technique is the cryoconcentration of the reactants in the unfrozen domains of the apparently frozen reaction system [6,7]. As illustrated in Scheme 1a, the reactants, namely the monomers (or polymers), cross-linker, and initiator are first dissolved in water to form a homogeneous aqueous solution at room temperature, and at a predetermined nominal monomer concentration C_{nom}, usually between 5 and 20%. The solution is then cooled to a sub-zero temperature, e.g., −18 °C. As water turns into ice, the reactants expel from the ice and cryoconcentrate in the unfrozen regions of the reaction system leading to the formation of a highly concentrated monomer solution surrounding the continuous ice phase (Scheme 1b). For instance, it was shown that the local concentration of *N*, *N*′-dimethylacrylamide monomer in the unfrozen zones at −20 °C is 45.5 wt%, which is 7.6-fold higher than its nominal concentration C_{nom} (6 wt%) [8]. Polymerization and cross-linking reactions ideally start with the aid of chemical or irradiated initiations. The resulting cryogels have ice domains acting as the template for the macropores surrounded by mechanically strong and elastic walls due to the high polymer concentration (Scheme 1c). Cryogelation provides a significant improvement in the properties of the hydrogels and organogels including permanent porosity, squeezability, poroelasticity, ultrafast responsivity, and a high-toughness [6,9–13]. The intensive research conducted in the past 10 years in the field of cryogels mainly focuses on the synthesis of novel synthetic or biopolymer cryogels without further considering the real conditions of the cryogelation system such as the real concentration of the monomers in the unfrozen domains and the ice volume determining the cryogel properties [14–16]. The questions that may arise are as follows: How does the local concentration of the reactants in the unfrozen regions vary depending on the type of the monomers or polymers? What kind of correlation exists between the ice volume in the cryogelation system and the pore volume of the cryogels? These are the questions we try to address in this study.

We prepared seven different cryogels under identical conditions, namely at −18 °C and at a fixed monomer (or polymer) concentration of 5 *w*/*v* %. Acrylamide (AAm), *N*, *N*-dimethylacrylamide (DMAA), sodium acrylate (NaAA), sodium methacrylate (NaMA), 2-acrylamido-2-methylpropane sulfonic acid sodium salt (AMPS) were selected as monomers while silk fibroin (SF), and double-stranded deoxyribonucleic acid

* Corresponding author.
E-mail address: okayo@itu.edu.tr (O. Okay).

https://doi.org/10.1016/j.reactfunctpolym.2023.105635
Received 16 April 2023; Received in revised form 21 May 2023; Accepted 2 June 2023
Available online 7 June 2023

(DNA) were the biopolymers for the preparation of cryogels. *N*, *N*′-methylenebisacrylamide (BAAm) and 1,4-butanediol diglycidyl ether (BDDE) were the chemical cross-linker for the preparation of synthetic and biopolymer cryogels, respectively. We should mention that AAm is a widely used hydrophilic and nonionic monomer while DMAA is a relatively hydrophobic nonionic monomer leading to the formation of associative polymers [17]. Moreover, hydrogels derived from NaAA and NaMA monomers are weak polyelectrolytes while those derived from AMPS are strong polyelectrolytes. SF is known to show extraordinary mechanical properties due to its β-sheet domains acting as physical cross-links [18]. Double stranded DNA is a semiflexible biopolymer and the hydrogels or cryogels derived from DNA exhibit smart functions such as self-healing, temperature sensitivity, selective binding, and molecular recognition [19]. The prediction of the morphological characteristics of the cryogels based on these monomers and polymers is thus important to obtain various tailor-made smart cryogels. Here, we investigate the effects of the chemical structure of the monomer units on the swelling, mechanical, and morphological properties of the resulting cryogels. The results are explained by considering the ice volume in the cryogelation system, and the true concentration of the monomers or polymers in the unfrozen domains, as determined by simple DSC measurements. Overall, this study highlights the importance of cryogenic conditions and chemistry in determining morphological and mechanical properties of cryogels.

2. Materials and methods

2.1. Materials

Acrylamide (AAm, Merck), *N*, *N*-dimethylacrylamide (DMAA, Sigma-Aldrich), acrylic acid (AAc, Merck), methacrylic acid (MAAc, Merck), 2-acrylamido-2-methylpropane sulfonic acid (AMPS, Sigma-Aldrich), *N*, *N*′-methylene bis(acrylamide) (BAAm, Merck), 1,4-butanediol diglycidyl ether (BDDE, Sigma-Aldrich), potassium persulfate (KPS, Fluka), sodium metabisulfite (SMS, Fluka), sodium bromide (NaBr, Merck) and *N*, *N*, *N*′, *N*′-tetramethylethylenediamine (TMEDA, Sigma-Aldrich) were used as received. Deionized water with a conductivity of 12.9 μS·cm^{-1} was used as the solvent for the cryogelation reactions, DSC solutions, and swelling measurements. AAc, MAAc, and AMPS were used after their neutralization with 1 M NaOH to pH = 7. Double-stranded deoxyribonucleic acid sodium salt (DNA) isolated from salmon testes was supplied from Sigma-Aldrich. Its molecular weight was 1.3 × 10^6 g·mol^{-1}, e.g., 2000 base pairs. Silk fibroin (SF) was extracted and purified from the cocoons of *Bombyx mori* (Kozabirlik, Turkey) as detailed before [20,21]. Briefly, the cocoons were boiled in an aqueous solution of 0.02 M Na_2CO_3 to remove sericin proteins from cocoons. The remaining SF was washed with water and then dissolved in aqueous 9.3 M LiBr solution for 2 h at 60 °C. The homogeneous SF solution was then dialyzed against pure water using 10,000 MWCO dialysis tubing (Snake Skin, ThermoFisher). The concentration of aqueous SF solution after dialysis was 9.1 wt%.

2.2. Cryogelation

The cryogelation reactions were conducted in a deep freezer at −18 °C for various times. It should be mentioned that −18 °C is the widely used subzero temperature for the cryogelation of aqueous reaction solutions. The initial cooling rate of the reaction solutions was of −2.0 ± 0.6 °C·min^{-1} (Fig. S1). The initial (nominal) concentration C_{nom} of the monomers and biopolymers was fixed at 5 *w*/*v* % throughout this study. The synthetic cryogels based on AAm, DMAA, NaAA, NaMAA, and AMPS were prepared using BAAm as a cross-linker at a molar ratio of 1/80 in the presence of 3 mM KPS and 0.25 *v*/v% TMEDA as the initiator and accelerator, respectively. For DMAA cryogels, SMS (1 mM) instead of TMEDA was used as an accelerator. Biopolymer cryogels based on SF and DNA were prepared using BDDE as a cross-linker in the presence of 0.25 *v*/v% TMEDA [22,23]. The amount of BDDE was fixed at 2 *w*/*v*% for DNA cryogel while for SF cryogel, 2.00 mL BDDE per gram SF, e.g., 20 mmole epoxide groups per gram of SF was used. The amounts of the cross-linker, initiator, and accelerator used in the cryogelation reactions were determined by considering our previous works [21–26], and preliminary experiments yielding a complete gel fraction.

Typically, to prepare cryogels based on AAm, AAm (0.5 g) was dissolved in 9.88 mL pure water in a glass vial, and then BAAm (13.6 mg) was added. After dissolution, 0.1 mL of 300 mM KPS stock solution and 0.025 mL TMEDA were added and stirred for a few seconds. The solution

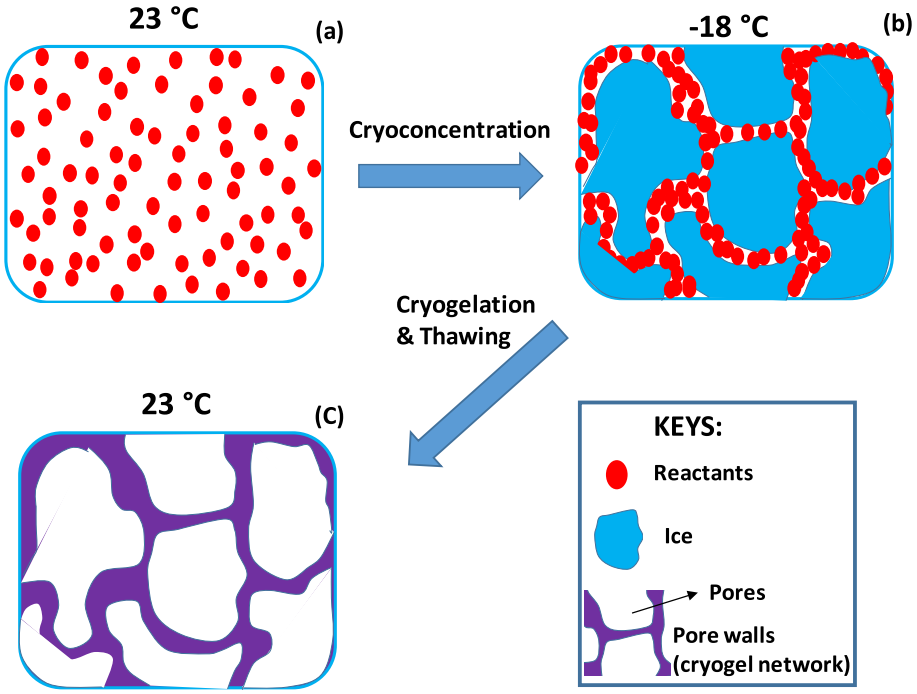

Scheme 1. Cartoon showing cryoconcentration of the reactants at −18 °C (a, b) followed by cryogelation and thawing to form a cryogel (c).

was then transferred into 1 mL plastic syringes and the cryogelation reactions were conducted at −18 °C. Cryogels based on DMAA, NaAA, NaMA, and AMPS were also prepared using the same procedure.

For the preparation of SF cryogels, 5.5 mL of 9.1 wt% aqueous SF solution was mixed in a glass vial with 3.5 mL pure water and 0.996 mL BDDE. After adding 0.025 mL TMEDA as a pH regulator [21], and stirring properly, the solution was transferred into 1 mL plastic syringes and cryogelation reactions were conducted at −18 °C. Cryogels based of DNA were prepared in 4 mM NaBr solution instead of water to prevent its denaturation [27]. Typically, 0.5 g DNA was dissolved in 4 mM aqueous NaBr solution at 35 °C for 1 day. 0.18 mL BDDE was then added and stirred at 35 °C for 1 h. After addition of 0.025 mL TMEDA, the solution was transferred into 1 mL plastic syringes of 4.5 mm internal diameter to conduct the cross-linking reaction at −18 °C.

2.3. Characterization of Cryogels

Preliminary experiments showed that all cryogels, except DNA, show a complete gel fraction after a reaction time of 24 h. In contrast, DNA needed at least 3 days to incorporate completely into the cryogel network. Therefore, the cryogelation time was fixed as 3 days for DNA, and 24 h for SF and the monomers. After cryogelation, the syringes containing cryogels were taken out of the deep freezer and submerged in an excess of water at 23 ± 2 °C for at least one week to remove soluble species. They were then dried in a freeze-dryer (Christ Alpha 2–4 LD-plus) using a three-step procedure involving freezing at −25 °C under atmospheric pressure for 24 h, main-drying at −40 °C under 0.12 mbar vacuum for 24 h, and final-drying at −60 °C under 0.011 mbar vacuum for 24 h. The gel fraction W_g which is the cross-linked polymer fraction obtained from monomer or polymer was calculated by the equation

$$W_g = \frac{m_{dry}}{m_0 w} \tag{1}$$

where m_{dry} is the weight of the dried cryogel, m_0 is the weight of as-prepared cryogel and w is the weight fraction of monomer or polymer in the cryogelation solution which was fixed at 0.05. The swelling behavior of cryogels was investigated in water which is a good solvent for all polymers. For this purpose, the freeze-dried cylindrical cryogels with 4.3 mm in diameter after preparation were cut into small samples with 2.5 ± 0.5 mm in thickness, and they were immersed in an excess of pure water. All cryogels attained their equilibrium swelling within less than 1 min. The equilibrium weight and volume swelling ratios, q_w and q_v, respectively, were calculated by,

$$q_w = \frac{m_{sw}}{m_{dry}} \tag{2a}$$

$$q_v = \left(\frac{D_{sw}}{D_{dry}}\right)^3 \tag{2b}$$

where m_{sw} and D_{sw} are the weight and diameter of the swollen samples in water, respectively, and D_{dry} is the diameter of the freeze-dried sample. All diameters were measured by absolute digimatic caliper (Mitutoyo) with 0–150 mm measurement range and 0.02 mm accuracy.

The total pore volume V_p, i.e., the volume of open pores in milliliters per gram of the freeze-dried cryogel was measured by immersing cryogel specimens in an excess of poor solvent until reaching equilibrium at room temperature. Because the poor solvent fills only the pores without penetrating into the polymer network, the mass increase of a freeze-dried cryogel specimen in a poor solvent gives the total pore volume, V_p. Methanol was chosen as a poor solvent for DNA cryogels while acetone was chosen for all other cryogels. The total pore volume was calculated by the equation

$$V_p = \frac{m_p - m_{dry}}{d_p\, m_{dry}} \tag{3}$$

where m_p is the weight of the samples in poor solvent, d_p is the density of poor solvent which is 0.784 and 0.792 g/mL for acetone and methanol, respectively. The texture determination of freeze-dried cryogels was carried out by optical microscopy and scanning electron microscopy measurements. An optical microscope (Olympus CX-31 microscope) was used to determine the interior structure of the cryogels in dry-state. All cryogels were cut into thin samples and then transferred to glass microscope slides. Their photographs were captured by Q Imaging Camera connected to a computer. Then, the average pore diameter of the cryogels was calculated from the images using Image-Pro Plus software. A scanning electron microscope (SEM, Quanta FEG 250) was also used to investigate the interior structure of the cryogels in dry-state under a high vacuum. After cryogel samples were coated with Au-Pd, SEM images were obtained for all cryogels at several magnifications between 50 and 1000 times. The average pore size in the SEM an OM images was estimated by analyzing at least 100 pores in the images taken at various magnifications.

2.4. Characterization of cryogelation solutions at −18 °C

The amount of unfrozen water, extent of cryoconcentration, and ice volume of the frozen solutions were determined by differential scanning calorimetry (Perkin-Elmer Diamond DSC 4000) under a nitrogen atmosphere. For this purpose, the cryogelation solutions were prepared as described above except that the initiator and catalyst were not added. The solutions, each 15 mg, were places in the aluminum pans of the instrument and they were frozen at −18 °C for 24 h. The pans were held in the instrument at −18 °C for 2 h and then heated from −18 to 10 °C with a scanning rate of 1 °C·min^{-1}. The ice melting temperature T_m in the presence of cryoconcentrated solutions was determined from the melting peaks according to ICTAC (International Confederation for Thermal Analysis and Calorimetry) standards. Thus, T_m was determined from the extrapolated peak onset temperature for water, DMAA, NaAA, NaMA and AMPS solutions, while the peak temperature was taken as the T_m for biopolymer (SF, DNA) solutions. Moreover, because of the existence of eutectic point in AAm solutions, the maximum of the second melting peak was taken as T_m for frozen AAm solutions. The melting enthalpy ΔH of frozen monomer/polymer solutions was determined from the area under the melting peak from DSC. The mass fraction f_{unf} of unfrozen water was calculated by the equation

$$f_{unf} = 1 - \frac{\Delta H}{\Delta H_m} \tag{4}$$

where ΔH_m is the melting enthalpy of ice taken as 333.89 J·g^{-1}. Cryoconcentration is, as detailed above, the phenomenon of increasing monomer concentration in cryogelation system due to the freezing of water. Thus, as water freezes, monomers or polymers accumulate in the still unfrozen domains until an equilibrium is obtained at a given subzero temperature. As a consequence, the local (true) concentration C_{true} of the monomers or polymers is always larger than their nominal concentration. It was calculated from the mass fraction f_{unf} of unfrozen domains by

$$C_{true} = \frac{C_{nom}}{C_{nom} + (1 - C_{nom}) f_{unf}} * 100 \tag{5}$$

where C_{nom} was fixed at 5 *w/v* % in our study. The ice volume of the frozen reaction solutions was calculated by the equation

$$V_{ice} = \frac{(1 - C_0)(1 - f_{unf})}{d_{ice} C_0} \tag{6}$$

where d_{ice} is the density of ice at −18 °C, 0.995 g/mL.

2.5. Statistical analysis

All the experimental data are the averages of three (for Wg) or eight independent measurements (for all other data). They are displayed in the form of the average value ± standard deviation (see Table S1-S4).

3. Results and discussion

Seven different cryogels based on AAm, DMAA, NaAA, NaMA, AMPS, SF and DNA were synthesized at −18 °C and at a fixed monomer (or polymer) concentration of 5 *w/v* %, the rest being water. This reveals the presence of around 95% ice during cryogelation, potentially acting as a template for the formation of pores. Moreover, because of the differences in the molar masses of the monomers, the monomer solutions have different molarities affecting the kinetics of the polymerization and/or cross-linking reactions. To eliminate this effect, a complete incorporation of the monomers and polymers into the 3D cryogel network was achieved by adjusting the reaction time. BAAm and BDDE were the chemical cross-linker for the preparation of synthetic and biopolymer cryogels, respectively. In the first subsection, we compare and discuss the swelling, morphological, and mechanical properties of the cryogels. The characteristics of the cryogelation solutions at −18 °C, namely the fraction of unfrozen water, the ice volume, and the true concentration of the reactants during cryogelation are then presented, and their effects on the cryogel properties are discussed in the second subsection.

3.1. Swelling, morphological, and mechanical properties of the cryogels

Except for the ionic cryogels based on AMPS and NaMA, all cryogels exhibited a gel fraction W_g close to unity indicating that the monomers or polymers are completely incorporated into the 3D cryogel network (Fig. S2). For AMPS and NaMA cryogels, W_g values are larger than unity reflecting the existence of bound water that cannot be removed after the freeze-drying procedure [28,29]. The filled and open bars in Fig. 1a present the equilibrium weight q_w and volume swelling ratios q_v, of the cryogels, respectively. The weight swelling ratio q_w of all cryogels is much larger than their volume swelling ratio q_v, and the difference between q_w and q_v increases in the order of SF < DMAA < AAm < DNA < NaAA <NaMA < AMPS. The larger weight swelling of cryogels can be explained with the water-filling of the pores of the cryogels when immersed in water during which their mass significantly increases without changing much their volume. Assuming isotropic swelling, q_v relates to q_w by [30],

$$q_v = \frac{d_0}{d_2}\left[1 + \frac{(q_w - 1)\, d_2}{d_1}\right] \tag{7}$$

where d_1 is the solvent density, d_2 is the bulk density of the polymer forming the pore walls, and d_o is the apparent density of dried cryogel which is inversely proportional to the dry-state porosity P by,

$$P = 1 - \frac{d_0}{d_2} \tag{8}$$

Eqs. (7), (8) reveal that the volume swelling ratio q_v assumes smaller values as the apparent density d_o decreases, i.e., as the porosity P increases. Combining Eqs. (7) and (8) gives a relation between the porosity P_{sw} of the swollen cryogels and their swelling ratios q_v and q_w [30],

$$P_{sw} = 1 - q_v\,[1 + (q_w - 1)d_2/d_1\,]^{-1} \tag{9a}$$

Assuming equal densities for polymer and water, Eq. (9a) reduces to

$$P_{sw} = 1 - \frac{q_v}{q_w} \tag{9b}$$

Thus, the difference between the weight or volume swelling ratios is directly proportional to the porosity P_{sw} of the swollen cryogels. The filled and open bars in Fig. 1b show the porosity P_{sw} calculated using Eqs. (9a) and (9b), respectively. Except SF with 86–90% porosity, all cryogels exhibit more than 95% porosity in their swollen states. The results also show that the simplified Eq. (9b) describes well the swollen state porosity of all cryogels. Another parameter reflecting the porous structure of cryogels is their total pore volume V_p in their dry states. This parameter was determined by immersing the freeze-dried cryogel specimens in a poor solvent that only enters into the pores without swelling the cryogel network. The pore volume V_p of all cryogels compiled in Fig. 2a shows that the nonionic monomers AAm and DMAA produce cryogels with the largest pore volumes (14–16 mL·g^{-1}). Moreover, although the ionic cryogels exhibit a high porosity P_{sw} in the swollen state (Fig. 1b), they have a smaller total volume of pores V_p, which is attributed to the collapse of the pores during drying, as verified

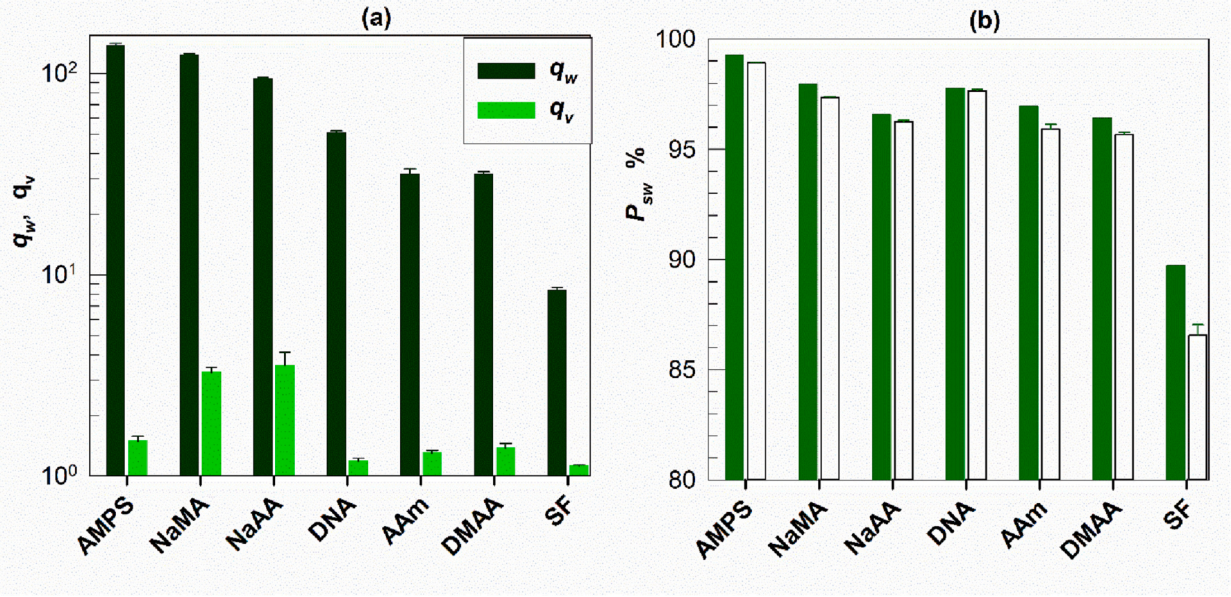

Fig. 1. (a) The equilibrium weight q_w and volume swelling ratios q_v of the cryogels. (b) Swollen state porosities P_{sw} of the cryogels. The filled and open bars show the porosity P_{sw} calculated using Eqs. (9a) and (9b), respectively, and using d_2 = 1.44, 1.35, 1.35, 1.21, 1.10, 1.29, and 1.05 g/mL for DNA, SF, and polymers of AAm, DMAA, NaAA, NaMA, and AMPS, respectively [22,31–33]. The data in (a) and (b) are arranged in decreasing order of q_w and P_{sw}, respectively.

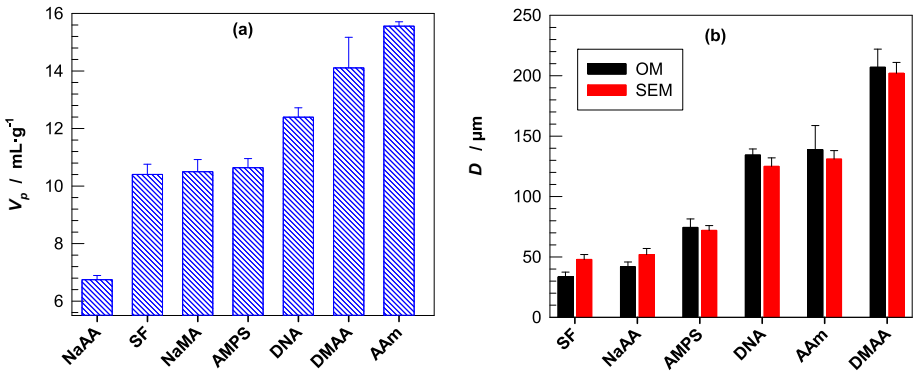

Fig. 2. Variations of the total pore volume V_p (a) and the average pore diameter D (b) depending on the type of the cryogels. The data in (a) and (b) are arranged in increasing order of V_p and D, respectively.

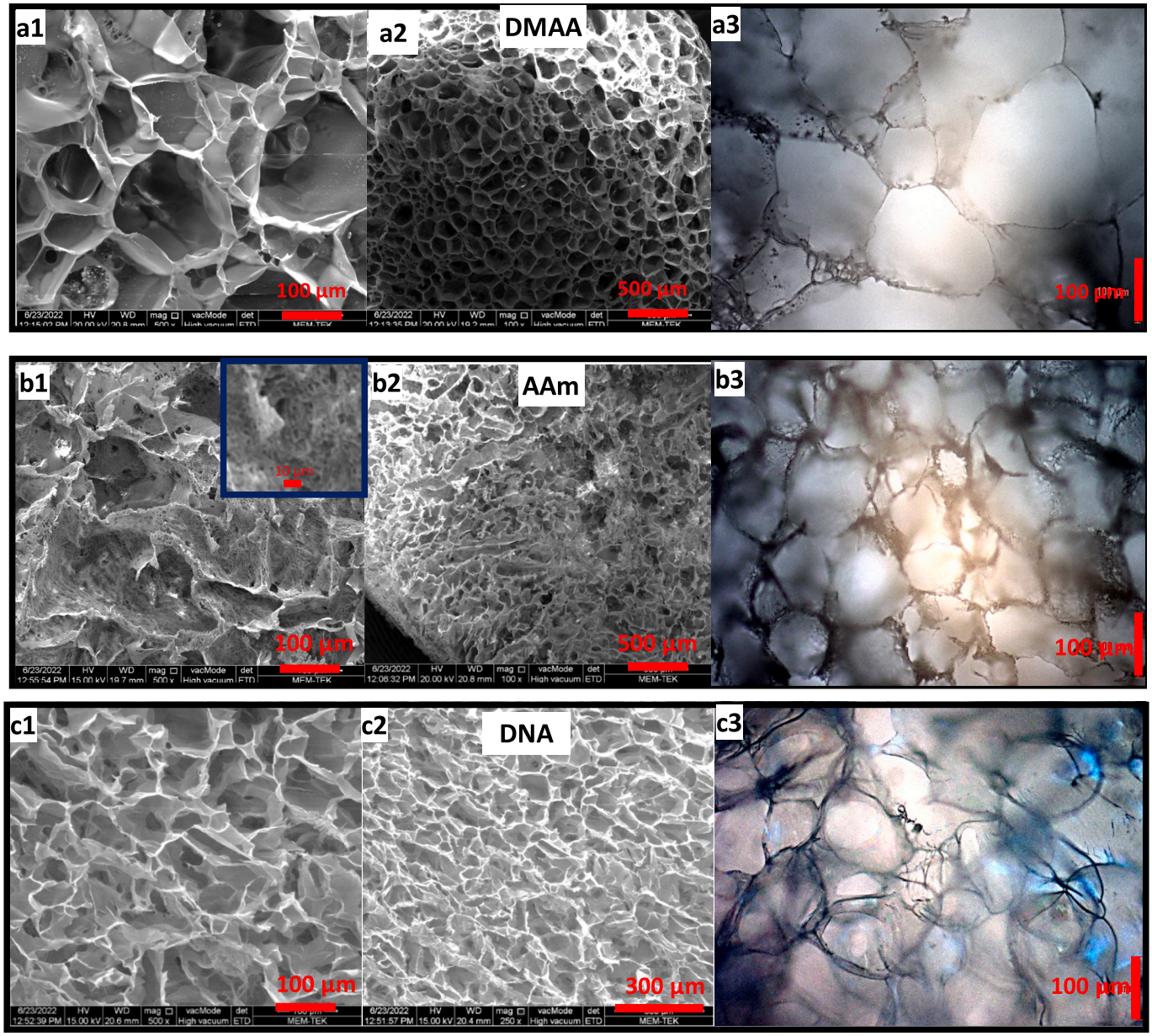

Fig. 3. SEM (first two columns) and OM images (last column) of cryogels based on DMAA (a1-a3), AAm (b1-b3), and DNA (c1-c3).

by morphological analysis.

The morphology of the cryogels was investigated by scanning electron microscopy (SEM) and optical microscopy (OM) measurements. Fig. 3 shows SEM (first two columns) and OM images (last column) of cryogels based on DMAA (a1-a3), AAm (b1-b3), and DNA (c1-c3) while the average pore diameter D of all cryogels are compiled in Fig. 2b. Moreover, SEM images of all cryogels at various magnifications are shown in Fig. S3. DMAA produces most regular and largest pores with an average diameter of around 200 μm. Both the diameter and regularity of the pores slightly decrease by replacing DMAA with AAm or DNA. Interestingly, AAm cryogel exhibits two generation of pores, namely in addition to the large pores of around 130 μm in diameter, small pores of a few μm in diameter appear in the walls of the large pores (inset to Fig. 3 b1). We attribute this characteristic of AAm cryogel to the bimodal melting behavior of aqueous AAm solution as will be discussed in the next section.

Fig. 4 shows SEM images of cryogels based on NaMA, AMPS, NaAA, and SF. The images reveal existence of irregular shapeless pores indicating collapse of the pores. Indeed, visual observation of these cryogels reflected shrinkage of the cryogel specimens after their freeze-drying. This could be related to the weak pore walls due to the low extent of cryoconcentration (see next section). Another reason is the existence of bound water acting as plasticizer in the cryogel structure so that the pore walls remain in the rubbery state facilitating collapse of the porous structure [34–36]. It was reported that the glass transition temperature T_g of polyacrylic acid decreases from 120 to around 25 °C with increasing water content to 15 wt% [36]. Thus, pore collapse induced by moisture absorption of ionic cryogels may also be responsible for their irregular pore structure. The average pore diameters determined from OM and SEM images also show that they can be varied over a wide range, i.e., between 30 and 200 μm, by changing the type of the cryogel (Fig. 2b).

To compare the mechanical properties of the cryogels, uniaxial compression tests were conducted on freeze-dried cryogel specimens in cylindrical shapes. We should note that NaMA, NaAA and AMPS cryogels collapse during drying and lose their cylindrical shapes so that the mechanical tests could not be conducted. Fig. 5a, b shows the stress-strain curves of dried cryogels in linear and semi-logarithmic scales, respectively. The compressive strengths of SF and AAm cryogels are 13.1 ± 0.7 and 3.1 ± 0.3 MPa, respectively, and clearly surpass those of other cryogels. Moreover, the cryogels except DNA exhibit a distinct plateau-like regime in the stress-strain curves during which they easily deform under an almost fixed stress. For instance, SF cryogel can easily be compressed from 10 to 40% strain under an almost constant stress of 0.72 ± 0.07 MPa. We can interpret this plateau as the transition region from linear to the hardening regimes as indicated by (1) and (2) in Fig. 5c, respectively. Thus, the porous structure of the cryogel remains intact in the linear regime while the pores start to collapse with the onset of the plateau. As the pores disappear and the cryogel turns into an almost nonporous one, the stress drastically increases in the final regime. The plateau stress can thus be interpreted as the stress required to break down the porous structure of the cryogels. Fig. 5b also reveals that SF cryogel has the most mechanically stable porous structure followed by AAm and DMAA cryogels. SF is known to show extraordinary mechanical properties due to its β-sheets domains acting as physical cross-links [22]. Although T_g of hydrophilic polymers decreases with increasing water plasticization, the water molecules in the amorphous regions of SF act as a plasticizer inducing β -sheet crystallization and hence further improving the mechanical properties [37]. Moreover, self-cross-linking ability of DMAA during cryopolymerization may also contribute to the mechanical strength of DMAA cryogels [38]. The mechanical tests were also conducted on AAm, AMPS and SF cryogels in their swollen states (Fig. S4). AAm and AMPS cryogel specimens can easily be compressed under less than 2 kPa stress up to 80% strain due to squeezing out water from the cryogel network. Finally, the steep increase at higher strains indicates compression of nearly nonporous AAm and AMPS networks. In contrast, SF cryogel in swollen state exhibits a plateau regime reflecting its mechanically stable porous structure, as in its dry state.

3.2. Effect of cryogenic conditions on the cryogel properties

The results presented above show that AAm, DMAA, and DNA create cryogels with a maximum pore volume in dry state and the largest pore diameters. They, together with the SF cryogel, also sustain large compressions without failure. In contrast, all ionic cryogels exhibit a low pore volume in dry state and irregular small pores due to the collapse of their porous structure. Moreover, from the studied cryogels, those based on silk fibroin (SF) was found to present the highest mechanical strength although they exhibit irregular and small pores. Thus, the cryogel properties significantly depend on the chemical structure of the cryogel scaffolds. This means that the nature of cryogel precursors under the cryogenic conditions should determine the properties of the cryogels. To highlight this effect, DSC measurements were conducted on the cryogelation solutions at −18 °C to determine the melting point of ice in the cryoconcentrated solutions, the amount of unfrozen water f_{unf}, the volume of ice V_{ice}, and the actual (true) concentration C_{true} of the cryogel precursors in the unfrozen domains of the cryogelation system. To determine the amount of unfrozen water at −18 °C, the cryogelation solutions containing 5 w/v % monomers or polymers, and the cross-linker were prepared without addition of the initiator and catalyst. After freezing the solutions at −18 °C, they were heated to 10 °C in a DSC instrument with a scanning rate of 1 °C·min^{-1} (Fig. 6a). Except AAm, all aqueous solutions of the monomers and polymers exhibited a single melting peak. As for the ionic monomers, melting point shifted to a lower temperature between −3 and − 7 °C because of their counterions (Fig. 6b). DSC analysis of AAm solution shows formation of a eutectic mixture that melted at −9.2 °C, as also reported before by Ivanov and Lozinsky [39]. Thus, in addition to the main melting peak at 1.2 ± 0.1 °C, a second melting peak at a much lower temperature appears in the aqueous AAm solutions. This means that the AAm solution exhibits two freezing temperatures leading to the formation of bimodal

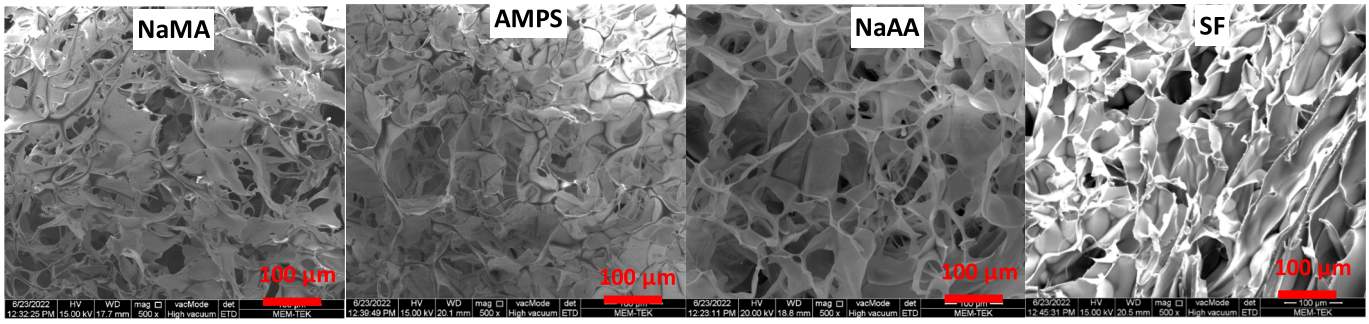

Fig. 4. SEM images of the cryogels based on NaMA, AMPS, NaAA, and SF.

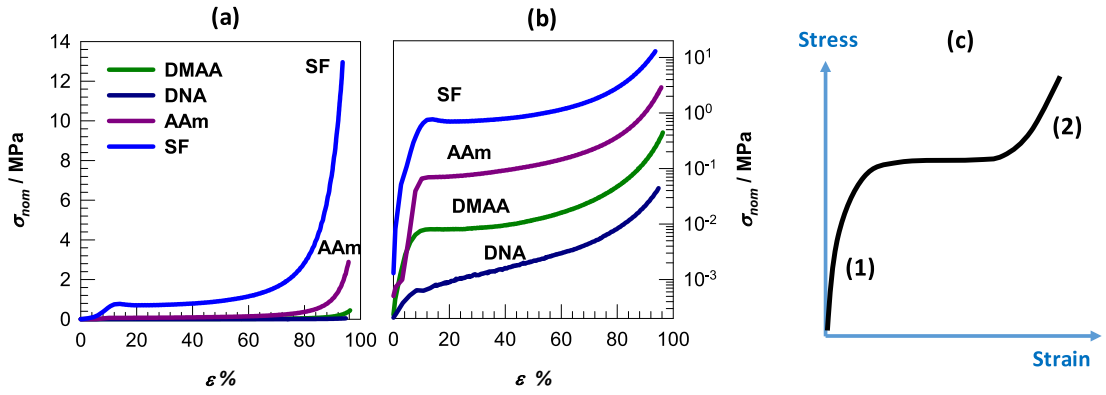

Fig. 5. (a, b) Stress-strain curves of the cryogels in linear (a) and semi-logarithmic scales (b). (c) Schematic presentation of the stress-strain curves for cryogels.

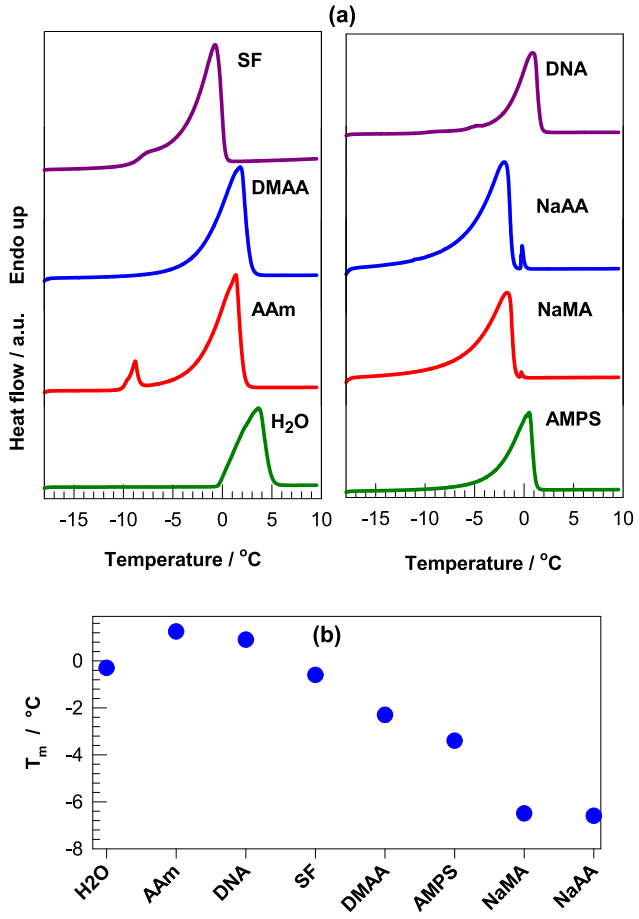

Fig. 6. DSC scans (a) and ice melting temperatures T_m (b) of bulk ice and in the presence of cryoconcentrated solutions of AAm, DMAA, NaAA, NaMA, AMPS, SF, and DNA at a fixed concentration of 5 *w/v* %.

pores in the resulting cryogels, as observed by SEM images (Fig. 3 b1).

Fig. 7a shows the variation of the fraction f_{unf} of unfrozen water at −18 °C depending on the type of the cryogels. f_{unf} varies between 6.5 ± 1 and 38 ± 1% depending on the type of the monomers or polymers. For the ionic monomers and polymers, more than 30% of water in the cryogelation system remains unfrozen at −18 °C while this amount decreases below 14% for the nonionic monomers DMAA and AAm. The lowest value of f_{unf} was found for DMAA as 6.5% which is attributed to its lower hydrophilicity. Fig. 7b shows the true concentration C_{true} of the monomers/polymers in the unfrozen domains. The nominal concentration C_{nom} of 5 *w/v* % was indicated by the horizontal dashed line. We should note that the C_{true}/C_{nom} ratio represents the extent of cryoconcentration under cryogenic conditions [5]. As expected from the large amount of unfrozen water in ionic cryogelation systems, the extent of cryoconcentration is not significant and C_{true}/C_{nom} ratio remains between 2.4 and 3.5. In contrast, this ratio increases for the nonionic monomers and SF because of its hydrophobic segments [18], and becomes 9 for DMAA corresponding a DMAA concentration of 45 w/v % in the unfrozen region. Because a higher C_{true} means a higher polymer concentration of the pore walls, the higher extent of cryoconcentration produces stable pore walls as observed for AAm and DMAA cryogels.

The filled symbols in Fig. 8 present the ice volume V_{ice} in the cryogelation system as estimated by DSC measurements. DSC data were converted to mL ice per gram of dry cryogel to make comparable with the experimental pore volume (V_p) data of the cryogels, as also shown in the figure by the bar plots. The general trend is that the ice volume V_{ice} calculated from the DSC results is larger than the pore volume V_p of the cryogels. This could be due to the partial collapse of the pores during drying of the cryogels. Moreover, in accord with the experimental V_p data, DSC simulations also predict that the nonionic monomers DMAA and AAm form cryogels with the largest ice volumes V_{ice}, namely 17.9 and 16.5 mL·g^{-1}, respectively. For other cryogels, V_{ice} remains almost constant at 13 ± 1 mL·g^{-1} indicating that the extent of pore collapse determines their V_p data. The results thus reveal that the measurement of the ice volume in the cryogelation solution is an effective tool to estimate the pore volume of the cryogels.

4. Conclusions

We presented the effects of cryogenic condition and chemistry on the properties of seven different cryogels prepared under identical conditions. The weight swelling ratio q_w of all cryogels is much larger than their volume swelling ratio q_v, and the difference between q_w and q_v corresponding to the swollen state porosity P_{sw} increases in the order of SF < DMAA < AAm < DNA < NaAA < NaMAA < AMPS. In their dry states, however, the nonionic monomers AAm and DMAA produce cryogels with the largest total pore volumes and average pore diameters while ionic cryogels exhibit a small pore volume due to the collapse of the pores during drying. Uniaxial compression tests reveal that SF cryogel has the most mechanically stable porous structure followed by AAm and DMAA cryogels. The experimental findings can be explained with the chemical structure of the cryogels as well as with the cryogenic conditions namely, the amount of unfrozen water f_{unf}, the volume of ice V_{ice}, and the true concentration C_{true} of the cryogel precursors in the unfrozen domains of the cryogelation system. It was found that the extent of cryoconcentration represented by the C_{true}/C_{nom} ratio is not significant for the ionic monomers and polymers, and remains between 2.4 and 3.5. This ratio increases for SF and the nonionic monomers, and becomes 9.0 for DMAA corresponding to 45 *w/v* % DMAA concentration in the unfrozen regions. Because a higher C_{true} means a higher polymer

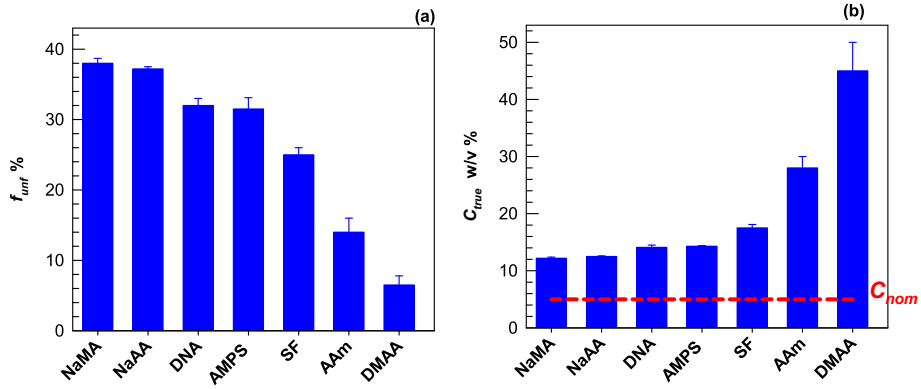

Fig. 7. Variations of the fraction of unfrozen water f_{unf} (a) and the true concentration C_{true} of the monomers/polymers in the unfrozen domains (b) at −18 °C depending on the type of the cryogels. C_{nom} of 5 w/v % was indicated by the horizontal dashed line in Fig. 7b. The data are arranged in decreasing order of f_{unf} (a) and increasing order of C_{true} (b).

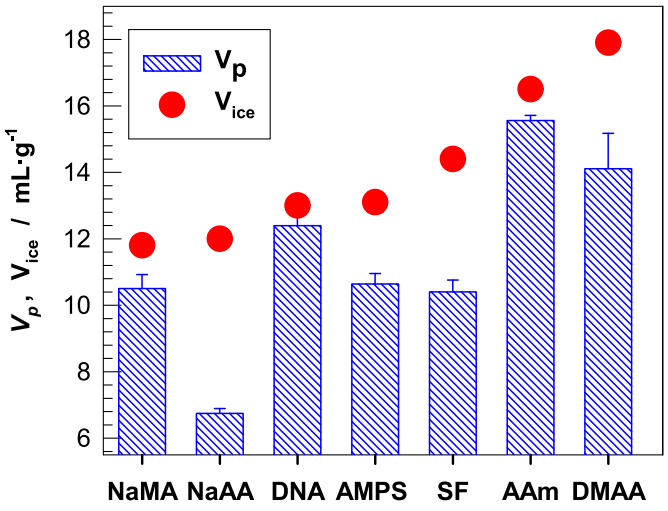

Fig. 8. The ice volume V_{ice} (filled symbols) in the cryogelation system estimated by DSC measurements. For comparison, the experimental pore volume data (V_p) of the cryogels are shown by the bar plots. The data are arranged in increasing order of V_{ice}.

concentration of the pore walls, the higher extent of cryoconcentration produces stable pore walls as observed for AAm and DMAA cryogels. In contrast, the pores in ionic cryogels easily collapse during drying due to the low C_{true}/C_{nom} ratio. Moreover, the general trend is that the ice volume V_{ice} calculated from the DSC results is larger than the pore volume V_p of the cryogels. This could be due to the partial collapse of the pores during drying of the cryogels. In accord with the experimental data, DSC simulations also predict that the nonionic monomers DMAA and AAm form cryogels with the largest ice volumes V_{ice}, namely 17.9 and 16.5 mL·g^{-1}, respectively, while for other cryogels, V_{ice} remains almost constant at 13 ± 1 mL·g^{-1}. The results thus reveal that the measurement of the ice volume in the cryogelation solution is an effective tool to estimate the pore volume of the cryogels.

Authors statement

The manuscript was written through contributions of all authors. All authors have given approval to the final version of the manuscript.

CRediT authorship contribution statement

Gamze Doser: Investigation, Data curation, Writing – original draft. **Esra Su:** Methodology, Data curation, Writing – review & editing. **Oguz Okay:** Conceptualization, Visualization, Methodology, Writing – review & editing.

Declaration of Competing Interest

The authors declare that they have no known competing financial interests or personal relationships that could have appeared to influence the work reported in this paper. We have no conflicts of interest to disclose.

Data availability

Data will be made available on request.

Acknowledgements

O.O. thanks Turkish Academy of Sciences (TUBA) for the partial support.

Appendix A. Supplementary data

Supplementary data to this article can be found online at https://doi.org/10.1016/j.reactfunctpolym.2023.105635.

References

[1] V.I. Lozinsky, Cryogels on the basis of natural and synthetic polymers: preparation, properties and application, Russ. Chem. Rev. 71 (2002) 489–511, https://doi.org/10.1070/RC2002v071n06ABEH000720.
[2] K.R. Hixon, T. Lu, S.A. Sell, A comprehensive review of cryogels and their roles in tissue engineering applications, Acta Biomater. 62 (2017) 29–41, https://doi.org/10.1016/j.actbio.2017.08.033.
[3] L.O. Jones, L. Williams, T. Boam, M. Kalmet, C. Oguike, F.L. Hatton, Cryogels: recent applications in 3D-bioprinting, injectable cryogels, drug delivery, and wound healing, Beilstein J. Org. Chem. 17 (2021) 2553–2569, https://doi.org/10.3762/bjoc.17.171.
[4] L.J. Eggermont, Z.J. Rogers, T. Colombani, A. Memic, S.A. Bencherif, Injectable cryogels for biomedical applications, Trends Biotechnol. 38 (2020) 418–431, https://doi.org/10.1016/j.tibtech.2019.09.008.
[5] A. Baimenov, D.A. Berillo, S.G. Poulopoulos, V.J. Inglezakis, A review of cryogels synthesis, characterization and applications on the removal of heavy metals from aqueous solutions, Adv. Colloid Interf. Sci. 276 (2020), 102088, https://doi.org/10.1016/j.cis.2019.102088.
[6] O. Okay, V.I. Lozinsky, Synthesis and structure–property relationships of cryogels, Adv. Polym. Sci. 263 (2014) 103–157, https://doi.org/10.1007/978-3-319-05846-7_3.
[7] V.I. Lozinsky, O. Okay, Basic principles of cryotropic gelation, Adv. Polym. Sci. 263 (2014) 49–102, https://doi.org/10.1007/978-3-319-05846-7_2.
[8] H. Kirsebom, G. Rata, D. Topgaard, B. Mattiasson, I.Y. Galaev, Mechanism of cryopolymerization: diffusion-controlled polymerization in a nonfrozen microphase, An NMR study. Macromolecules 42 (2009) 5208–5214, https://doi.org/10.1021/ma900566d.

[9] B. Yetiskin, O. Okay, A silk fibroin cryogel building adaptive organohydrogels with switching mechanics and viscoelasticity, ACS Appl. Polym. Mater. 4 (2022) 5234–5245, https://doi.org/10.1021/acsapm.2c00741.
[10] M.N. Guven, G. Demirci, S. Altuncu, U. Gulyuz, O. Okay, H.Y. Acar, D. Avci, Alendronate-functionalized poly(amido amine) cryogels of high-toughness for biomedical applications, Polymer 190 (2020), 122248, https://doi.org/10.1016/j.polymer.2020.122248.
[11] B. Tavsanli, O. Okay, O., Macroporous hyaluronic acid cryogels of high mechanical strength and flow-dependent viscoelasticity, Carbohydr. Polym. 229 (2020), 115458, https://doi.org/10.1016/j.carbpol.2019.115458.
[12] S. Muslumova, B. Yetiskin, O. Okay, Highly-stretchable and rapid self-recoverable Cryogels based on butyl rubber as reusable sorbents, Gels 5 (2019) 1, https://doi.org/10.3390/gels5010001.
[13] B. Yetiskin, O. Okay, High-strength and self-recoverable silk fibroin cryogels with anisotropic swelling and mechanical properties, Int. J. Biol. Macromol. 122 (2019) 1279–1289, https://doi.org/10.1016/j.ijbiomac.2018.09.087.
[14] M.V. Dinu, M.M. Ozmen, E.S. Dragan, O. Okay, Freezing as a path to build macroporous structures: superfast responsive polyacrylamide hydrogels, Polymer 48 (2007) 195–204, https://doi.org/10.1016/j.polymer.2006.11.022.
[15] E. Su, O. Okay, Cryogenic formation-structure-property relationships of poly(2-acrylamido-2-methyl-1-propanesulfonic acid) cryogels, Polymer 178 (2019), 121603, https://doi.org/10.1016/j.polymer.2019.121603.
[16] E.S. Dragan, M.M. Lazar, M.V. Dinu, F. Doroftei, Macroporous composite IPN hydrogels based on poly(acrylamide) and chitosan with tuned swelling and sorption of cationic dyes, Chem. Eng. J. 204–206 (2012) 198–209, https://doi.org/10.1016/j.cej.2012.07.126.
[17] L. Weng, A. Gouldstone, Y. Wu, W. Chen, Mechanically strong double network photocrosslinked hydrogels from N,N-dimethylacrylamide and glycidyl methacrylated hyaluronan, Biomaterials 29 (2008) 2153–2163, https://doi.org/10.1016/j.biomaterials.2008.01.012.
[18] H.-J. Jin, D.L. Kaplan, Mechanism of silk processing in insects and spiders, Nature 224 (2003) 1057–1061, https://doi.org/10.1038/nature01809.
[19] O. Okay, DNA hydrogels: new functional soft materials, J. Polym. Sci. B Polym. Phys. 49 (2011) 551–556, https://doi.org/10.1002/polb.22213.
[20] U.J. Kim, J. Park, C. Li, H.J. Jin, R. Valluzzi, D.L. Kaplan, Structure and properties of silk hydrogels, Biomacromolecules 5 (2004) 786–792, https://doi.org/10.1021/bm0345460.
[21] I. Karakutuk, F. Ak, O. Okay, Diepoxide-triggered conformational transition of silk fibroin: formation of hydrogels, Biomacromolecules 13 (2012) 1122–1128, https://doi.org/10.1021/bm300006r.
[22] F. Ak, Z. Oztoprak, I. Karakutuk, O. Okay, O. Macroporous silk fibroin cryogels, Biomacromolecules 14 (2013) 719–727, https://doi.org/10.1021/bm3018033.
[23] P. Karacan, H. Cakmak, O. Okay, Swelling behavior of physical and chemical DNA hydrogels, J. Appl. Polym. Sci. 128 (2013) 3330–3337, https://doi.org/10.1002/app.38550.
[24] P. Karacan, O. Okay, Ethidium bromide binding to DNA cryogels, React. Funct. Polym. 73 (2013) 442–450, https://doi.org/10.1016/j.reactfunctpolym.2012.11.014.
[25] C. Bilici, S. Karayel, T.T. Demir, O. Okay, Self-oscillating pH-responsive cryogels as possible candidates of soft materials for generating mechanical energy, J. Appl. Polym. Sci. 118 (2010) 2981–2988, https://doi.org/10.1002/app.32693.
[26] D. Ceylan, M.M. Ozmen, O. Okay, Swelling-deswelling kinetics of poly(acrylamide) hydrogels and cryogels, J. Appl. Polym. Sci. 99 (2006) 319–325, https://doi.org/10.1002/app.22023.
[27] F. Topuz, O. Okay, Rheological behavior of responsive DNA hydrogels, Macromolecules 41 (2008) 8847–8854, https://doi.org/10.1021/ma801414p.
[28] S. Durmaz, O. Okay, O., Acrylamide/2-acrylamido-2-methyl propane sulfonic acid sodium salt-based hydrogels: synthesis and characterization, Polymer 41 (2000) 3693–3704, https://doi.org/10.1016/S0032-3861(99)00558-3.
[29] V.M. Gun'ko, I.N. Savina, S.V. Mikhalovsky, Properties of water bound in hydrogels, Gels 3 (2017) 37, https://doi.org/10.3390/gels3040037.
[30] O. Okay, Macroporous copolymer networks, Prog. Polym. Sci. 25 (2000) 711–779, https://doi.org/10.1016/S0079-6700(00)00015-0.
[31] M. Ilavsky, Phase transition in swollen gels. 2. Effect of charge concentration on the collapse and mechanical behavior of polyacrylamide networks, Macromolecules 15 (1982) 782–788, https://doi.org/10.1021/ma00231a019.
[32] N. Orakdogen, O. Okay, Reentrant conformation transition in poly(N,N-dimethylacrylamide) hydrogels in water-organic solvent mixtures, Polymer 47 (2006) 561–568, https://doi.org/10.1016/j.polymer.2005.11.066.
[33] Y. Liu, Y. Han, Y. Wu, L. Xiong, T. Hang, H. Ling, A. Hu, L. Gao, L.M. Li, Grafting of poly(methacrylic acid-co-acrylamide) film on silicon surface via a simultaneous hydrolysis process, Mater. Today Commun. 21 (2019), 100678, https://doi.org/10.1016/j.mtcomm.2019.100678.
[34] H.K. Yuen, E.P. Tam, J.W. Bulock, On the glass transition of polyacrylamide, in: S. F. Johnson, P.S. Gill (Eds.), Analytical Calorimetry vol. 5, Plenum Press, New York, 1984, pp. 13–24.
[35] G.I. Tsereteli, T.V. Belopolskaya, N.A. Grunina, O.L. Vaveliouk, Calorimetric study of the glass transition process in humid proteins and DNA, J. Therm. Anal. Calorim. 62 (2000) 89–99, https://doi.org/10.1023/A:1010110727782.
[36] H. Xu, L. Guan, Investigation on the heat capacity of water in poly(acrylic acid)/water mixtures through stepscan method, J. Macromol. Sci. B. Physics 50 (2011) 956–966, https://doi.org/10.1080/00222348.2010.497102.
[37] K. Yazawa, K. Ishida, H. Masunaga, T. Hikima, K. Numata, Influence of water content on the b-sheet formation, thermal stability, water removal, and mechanical properties of silk materials, Biomacromolecules 17 (2016) 1057–1066, https://doi.org/10.1021/acs.biomac.5b01685.
[38] O.E. Zaborina, R.G. Gasanov, A.S. Peregudov, V.I. Lozinsky, Eur. Polym. J. 61 (2014) 226–239, https://doi.org/10.1016/j.eurpolymj.2014.10.006.
[39] R.V. Ivanov, V.I. Lozinsky, Cryopolymerization of acrylamide: Effect of thermal history of a moderately frozen reaction system, Polym. Sci. Ser. A 48 (2006) 1231–1239. ISSN 0965-545X, Original Russian Text: R. V. Ivanov, V. I. Lozinsky, Vysokomolekulyarnye Soedineniya, Ser. A, 2006, 48 (2006) 2092–2101.